



Two-dye two-color laser-induced fluorescence spectroscopy on droplets of green solvent water/ethanol mixtures for thermometry and mixture composition

Hannah Ulrich^{1,2} · Richard Weiß¹ · Lars Zigan^{1,2}

Received: 24 May 2024 / Revised: 2 August 2024 / Accepted: 7 August 2024
© The Author(s) 2024

Abstract

This work shows new insights on the application of two-color laser-induced-fluorescence (2c-LIF) thermometry in a droplet chain. A two-dye mixture is used in ethanol, water and ethanol/water mixtures in order to reach a high-temperature sensitivity and avoid the detection of lasing effects in the droplets. Various droplet sizes are recorded in regard to the limitation of the detection system for very small micrometric droplets. The breakup of a droplet chain is measured to assess the spectral detection system in applications with liquid structures of different sizes. Additionally, a proposal to expand the 2c-LIF application for studying ethanol/water droplets regarding mixture composition with a third color channel is presented. Forming two intensity ratios, the spectra can be used to obtain information on the mixture composition of the solvent. Measurements in different ethanol/water mixtures containing 0–100 vol% water are evaluated to show this possibility.

1 Introduction

Determining “responsible consumption and production” as one of the United Nations’ goals for sustainable development, a specific focus was set on chemicals and waste. This goal is mainly addressed to the industry, having a significant potential for climate-friendly changes. In order to reach a higher sustainability in technical applications, the utilization of green solvents is decisive. Water and ethanol substitute more complex solvents, showing advantages like ecological manufacturing, reusability or biodegradation, as well as reduced health and safety risks (Capello et al. 2007; Chemat et al. 2019). Both liquids and their mixtures are found in various industrial areas, being used in spray or film cooling (Bhatt et al. 2017; Najim et al. 2020), as coolants in electro-sprays for high power density devices (Taheri et al. 2024), or in regular adsorption coolers (Dzigbor and Chimphango 2019; Lache et al. 2023). Many other fields of applications

for the solvent mixtures can be named, ranging from a use as biofuel additives or ethanol fuel blends (Qi et al. 2010) or as solvents for extraction in pharmaceutical, medical or food industries (Amyrgialaki et al. 2014; Monroy et al. 2016; Mylonaki et al. 2008; Plaskova and Mlcek 2023; Zhang et al. 2007). Regarding the development and optimization of these solvent-based industrial processes, important variables are the liquid phase temperature and also the mixture fraction. Therefore, the focus of this work is the limitations and opportunities of two-dye 2c-LIF measurements in droplets, as the basic thermometry concept was presented in our recent work (Ulrich et al. 2023). Investigations are extended to measurements in ethanol, water and their mixtures, especially for very small droplets and atomizing jets.

2c-LIF allows the temperature determination in liquid flows or two-phase flows, e.g. dense and dilute sprays (Düwel et al. 2007; Mishra et al. 2016; Prenting et al. 2020) or liquid films (Collignon et al. 2021, 2022; Koegl et al. 2024). By admixing a temperature-sensitive fluorescent dye to the liquid, an emission signal ratio can be detected and used to infer the temperature. The ratio is formed from the signals of two wavelength areas of the emission spectrum of the dye. Ideally one of these color bands maps a temperature-sensitive, and the other band an oppositely sensitive or temperature-insensitive spectral excerpt. The selection of these spectral bands by respective filters may lead to a higher-temperature sensitivity of the signal ratio. In case

✉ Hannah Ulrich
hannah.ulrich@unibw.de

¹ Institut für Thermodynamik, Professur für Energiewandlung, Fakultät für Luft- und Raumfahrttechnik, Universität der Bundeswehr München (UniBw M), Neubiberg, Germany

² Erlangen Graduate School in Advanced Optical Technologies (SAOT), Friedrich-Alexander-Universität Erlangen-Nürnberg (FAU), Erlangen, Germany

of evaporation, a related change in dye concentration in the liquid probe can result in self- or reabsorption of the fluorescence signal by other dye molecules. Approaching the 2c-LIF technique with two different dyes (two-dye two-color LIF) allows for a wider selection of color channels to form a maximum temperature-sensitive signal ratio. Additionally, the influence of solvent evaporation on the signal reabsorption and resulting signal ratio can be reduced. Therefore, the selection of the dyes and the accompanying filter set is conducted in consideration of the overlap of absorption and emission spectra.

Several authors characterized different fluorescent dyes for the use of liquid phase thermometry in cuvettes (Mishra et al. 2020; Prenting et al. 2020). To the authors best knowledge, Chaze et al. (2016) were first to propose the dye mixture of fluorescein (FL) and sulforhodamine 101 (SRh) in water for 2c-LIF thermometry. Temperature fields of a heated water jet are measured by injecting into stationary water doped with the dye mixture. In a further study, temperatures of millimetre-sized water droplets impinging on a hot surface were investigated (Chaze et al. 2017). The use of this dye mixture was adopted by Collignon et al. (2021) to study the temperature distribution in wavy liquid films. Earlier works presented thermometry in single droplets, studying rhodamine dyes with a PMT (photomultiplier tube) detection system (Castanet et al. 2003; Lavieille et al. 2001; Maqua et al. 2006). Evaporation measurements of millimetre-sized droplets doped with rhodamine were conducted with imaging systems for two-color LIF thermometry (Strizhak et al. 2018; Volkov and Strizhak 2020). Droplet images were shown with a minimum droplet size of around 0.5 mm (Volkov and Strizhak 2020). In our previous work, the dye combination of FL and SRh was used for temperature calibration and evaporation studies in 100 μm sized ethanol droplets in a monodisperse droplet chain (Ulrich et al. 2023). An imaging and a spectral detection system were used to record the fluorescence emission. Investigations of the detection limitation in regard to small μm -size droplets are a focus of the present work. Although there are liquid temperature measurements based on 2c-LIF in sprays available in the literature as mentioned above, there are few papers available on thermometry in individual μm -sized droplets (e.g. Palmer et al. 2016 in droplets with diameter of 67 μm). Because of the polydisperse nature of sprays, it is not clear, whether the smallest droplets can be detected at all. This is because the LIF signal roughly depends on the volume of the droplet and thus larger droplets in sprays dominate the signal intensity distribution, while signals of small droplets in dense sprays may be lost (Storch et al. 2016b). Additionally, there are challenges for laser diagnostics in droplets because of lens effects (Ulrich et al. 2023). This leads to “dead zones” in the LIF signal, appearing due to light refraction and convergence (Volkov and Strizhak 2020). These optical effects

may also be present in the non-spherical structures during breakup and need further investigation (Ulrich et al. 2023). Other effects are bright signals due to dye lasing or so-called morphology-dependent resonances (MDR, or sometimes named “whispering gallery modes”, WGM) occurring at the phase boundary of the droplet. These optical effects are present in sprays as well, but may not be detected due to the limited resolution of the optical setup. However, these effects may bias the fluorescence signals and derived quantities such as temperature, droplet size (e.g. in planar droplet sizing based on LIF/Mie ratio) or concentration.

As mixture composition is another relevant variable in the solvent industry, the application of 2c-LIF with the proposed dyes is considered for composition measurements in water/ethanol mixtures. The dependency of the fluorescence signal and its spectral shift in various solvents is known for many dyes, e.g. for Rhodamine 6G (Zehentbauer et al. 2014) or Coumarin 152, Rhodamine B and Pyrromethene 597 (Prenting et al. 2020). However, such fluorophores were rarely applied for composition measurements in, e.g. binary liquid mixtures. Storch et al. (2016a) applied triethylamine (TEA) in different liquid ethanol/isooctane fuel blends and observed a shift of the fluorescence spectrum towards larger wavelength with increase in ethanol content. However, the signal for large ethanol concentrations (85% and 100%) was extremely low. Koegl et al. (2022) proposed the dye Nile Red for composition determinations of isooctane/ethanol mixtures (for ethanol volume fractions between 0% and 100%) with a 2c-LIF concept. A similar approach was applied for fuel mixtures of n-decane and butanol (Koegl et al. 2020b). Maqua et al. (2006) added another color channel to apply 3c-LIF with the dye Rhodamine B for thermometry in binary ethanol/acetone droplets with varying compositions (Maqua et al. 2006). A red-shift of the emission spectrum of Eosin-Y fluorescence was observed for the solvent ethanol compared to water (Koegl et al. 2020c). Although LIF was proposed for studying water/fuel emulsions for addition of ethanol (Koegl et al. 2020a), there is no LIF technique available for composition measurements of liquid binary ethanol/water mixtures until now. Other diagnostics based on light scattering (Raman, rainbow refractometry, etc.) for studying droplet compositions are reviewed by Lemoine and Castanet (Lemoine and Castanet 2013).

In the present work, the two-dye two-color LIF imaging system with two sCMOS cameras is utilized for the determination of droplet sizes, as well as for a visualization of jet breakup and optical processes inside liquid structures and droplets. For a better insight into optical effects, like MDR and the avoidance of their detection, simultaneous spectral measurements are conducted with a VIS spectrometer. Furthermore, these measurements provide a simple and quick solution to compare spectra and to recognize effects like spectral shifts depending on temperature and

composition. Due to fibre couplings and their flexible and compact sizing, the application and post-processing of spectral measurements for LIF is more feasible and favourable than imaging systems, especially in case of limited optical access. Therefore, the main focus in this paper lies on the spectrally detected fluorescence emission. Additionally, the data to verify the size limitation is recorded in several ethanol/water mixtures. This demonstrates the usability of the selected dye combination in different solvents. Important factors are the solubility of the dyes, the excitation at 532 nm and the temperature-dependent behaviour of the dye/solvent mixture.

2 Materials and methods

This section contains an abridgement of LIF fundamentals and the experimental setup. 2c-LIF techniques are based on the photo-physics of organic dyes, diluted in the respective solvent. Due to the absorption of photons of the laser wavelength (here 532 nm), the dye molecules are excited to an elevated energetic state. Fluorescence describes the process of spontaneous light emission of the excited molecule, to lose this excess energy and reach its' energetic ground state again. Transitional processes reduce the emitted energy, which leads to a reduction and an according Stokes shift (red-shift) of the fluorescence signal, compared to the absorbed wavelength (Schulz and Sick 2005). The emitted spectrum may also be sensitive to parameters, e.g. temperature. In this case, a temperature change leads to a different energetical distribution of the dye molecules over vibrational or rotational energy levels. The Boltzmann distribution describes this population dispersion and can lead to a temperature-sensitive shift of the spectrum (Bräuer 2015). A detailed discourse regarding the theory of 2c-LIF and the applied two-dye concept can be found in the authors previous work (Ulrich et al. 2023).

Using a signal ratio R_{fl} of two fluorescence intensities I_{fl} , the 2c-LIF approach eliminates the influence of several variables. Both fluorescence intensities I_{fl} represent a signal, simultaneously detected in a respective wavelength band.

Each wavelength band depicts a section of the two-dye fluorescence emission spectrum. In the linear range of the laser fluence, the emission signal ratio is expressed as

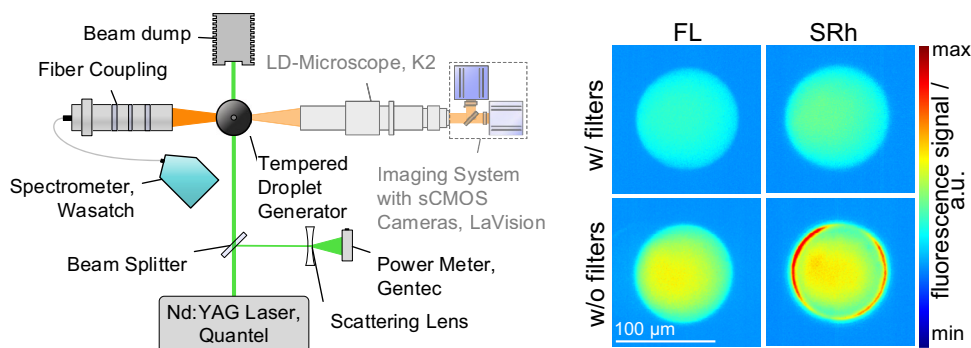
$$R_{fl} = \frac{I_{fl,1}}{I_{fl,2}} = \frac{K_{opt,1}(\lambda)K_{spec,1}(\lambda)I_0VCe^{\beta_1(\lambda)/T}}{K_{opt,2}(\lambda)K_{spec,2}(\lambda)I_0VCe^{\beta_2(\lambda)/T}} = \frac{K_{opt,1}K_{spec,1}}{K_{opt,2}K_{spec,2}} e^{\frac{\beta_1-\beta_2}{T}}$$

while β/K , K_{spec}/mol^{-1} and $K_{opt}(\lambda)$ — are wavelength-dependent constants (Lemoine et al. 1999). β and K_{spec} characterize physical and fluorescent properties of the predominating dye (Perrin et al. 2015). The detection systems' efficiency is described by K_{opt} . Building a ratio, the influence of the laser fluence I_0 , the liquid volume V/m^3 and the dye concentration $C/\text{mol}\cdot\text{m}^{-3}$ is eliminated. Furthermore, the dependencies on the constants K_{spec} and K_{opt} are eliminated, normalizing the ratio to a reference measurement.

The 2c-LIF approach is based on the admixture of a fluorescent dye to the investigated fluid. In our work, water and ethanol (EtOH) are studied, as well as their mixtures in several compositions (EtOH0 to EtOH100). These are referred to by their volume fraction of ethanol. A mixture of two dyes, FL (CAS: 518-47-8) and SRh (CAS: 60311-02-6), with a mass ratio of 10:1 (750 mg_{FL}/l and 75 mg_{SRh}/l) is diluted in all respective solvents. Therefore, a higher-temperature sensitivity can be achieved as with the use of only one dye. Furthermore, fluorescence reabsorption by the respective dye molecules itself can be avoided, taking the absorption spectra into account. With the proposed mixture and filter combination in the detection system, the recording of MDR, leading to very high LIF signals on the droplet rim, can be circumvented.

To measure the addressed two-dye fluorescence emission spectrum, an experimental setup is equipped with a fibre-coupled spectrometer to deliver spectral information, as depicted in Fig. 1 (left). A monodisperse droplet chain with droplet sizes from 30 to 120 μm is generated by a piezoelectrically controlled droplet generator (FMAG 1520, TSI). The tempered droplet generator is assembled with a compressed air supply and a syringe pump (AL1000-220, Aladdin), containing a mixture of solvent and fluorescent dyes. Producing droplets of various sizes, the liquid flow

Fig. 1 Left: Optical setup with spectral detection of the fluorescence emission around a heated droplet generator. Right: Example single-shot LIF images of FL and SRh emissions with respective BP filters (top row) and without BP filters (bottom row). Measurements are for ethanol at 293 K



rate is varied between 2 ml/h and 70 ml/h and the applied frequency of the ultrasound actuator between 20 and 50 kHz. The tempered and dry focussing air for droplet formation, which also shields the droplets at the nozzle exit against ambient air, comes from a compressor system with at least 253 K pressure dewpoint corresponding to a water vapour pressure of a maximum of 0.5204 Pa. Later on, droplets mix with ambient air, while temperature and humidity are constantly measured with a thermo-hygrometer in the laboratory. To illuminate the fluorescent mixture at 532 nm, a pulsed Nd:YAG laser (Q-SMART 850, Quantel) is being operated with a frequency of 10 Hz and a fluence of 2.4 mJ/cm². The laser beam has a diameter of 8 mm and is led through the droplet chain into a beam dump.

Orthogonally to the laser beam, an imaging system is mounted for size calibration. This system contains a long-distance microscope (Infinity DistaMax, K2), followed by a dichroic mirror (T588lpxr, Chroma), to separate the signal at 588 nm. The separated wavelength bands are each detected by sCMOS camera (Imager, LaVision) after passing specifically selected bandpass filters (554/23 BrightLine HC and 615/24 BrightLine HC). Images of recorded droplet fluorescence with (top) and without (bottom) these bandpass filters can be seen in the right image in Fig. 1. The picture shows droplets as seen by the two different cameras, after the signal has passed the dichroic mirror. As expected, the signal without the filters is higher, than with the filters mounted in front of each camera. Without the filter mounted to the camera, detecting the SRh signal, strong LIF signals due to MDR occur on the droplet surface.

The investigation of the spectral location of the MDR is performed with another detection system mounted at 90° to the laser beam. A spectrometer (WP-VIS-A-S-50, Wasatch Photonics) is fibre-coupled to an optical system, consisting of a notch filter and two achromatic doublets. Thus, spectral information is obtained, clarifying the wavelength position of the disturbing MDR signal. The spectrometer setup has the advantage of a small dimension, a moveable mounting and a lower cost than the camera system. The recorded data of the spectrometer requires only little memory space and allows for simplified post-processing. Therefore, even technical systems with, e.g. limited optical accessibility can be investigated with this setup. A comparison of the signals detected with the imaging and the spectrometer setup showed very similar results for the signal ratios and resulting temperature calibration curve (Ulrich et al. 2023). In this work, LIF images are only provided for droplet visualization and a better understanding of breakup processes of the jet and occurring lasing effect. All spectra are obtained by five recordings of 100 averaged single spectra per measurement location (as specified below), each with an integration time of 50 ms. Background measurements are subtracted from the spectra and a baseline fit is conducted. The single

intensity signals, forming the signal ratio, are the integrated emission signals in the respective color channel region of the fluorescence spectra.

Additional absorption measurements are conducted with an UV/VIS-spectrophotometer (V-750, Jasco). A tempered cuvette holder allows the recording of temperature-dependent absorption spectra. Due to a larger path length in the cuvette, a more diluted mixture (50 mg_{FL}/l and 5 mg_{SRh}/l) is prepared. This data is recorded to extend the understanding of the interaction of the dyes in different solvents. All temperature-dependent measurements are limited to a maximum temperature of 343 K, due to the boiling point of ethanol.

3 Results and discussion

The following section shows absorption and emission spectra of the dye mixture in different solvents. Absorption spectra are discussed with respect to the temperature dependence. Investigations of the fluorescence emission spectra are conducted to determine the lower signal limit of the detection systems regarding droplet sizes. Furthermore, the impact of structure size, also considering MDR signals, on the signal ratio and the subsequent temperature sensitivity is examined. Additional studies based on the spectral LIF detection system are conducted for various liquid mixtures and temperatures. Furthermore, the setup is applied to measure the temperature evolution downstream an atomizing jet, produced in the droplet generator. Spray-like liquid structures are produced, testing the suitability for detection of various droplet sizes, moving inside and outside the focus. Finally, the established 2c-LIF approach is analysed regarding an application to measure solvent compositions. For this purpose, an improved 3c-LIF method is proposed.

3.1 Absorption spectroscopy

Figure 2 shows the temperature-dependent evolution of the photon absorption in pure water—EtOH0, a mixture of 40 vol% ethanol and 60 vol% water—EtOH40 and pure ethanol—EtOH100, as well as the laser line at 532 nm. With the absorption spectrophotometer, six different ethanol–water mixtures (20 vol% steps) were measured in 10 K intervals from 283 K (marked with “c”-cold) to 343 K (“h”-hot). All measured spectra allow a clear differentiation between one absorption spectrum due to FL at wavelengths from 410 to 540 nm and another due to SRh, around 555 to 610 nm. In cold conditions, FL absorbs more light, the higher the water fraction. Additionally, a blue-shift of the peak can be observed, which is a possible explanation for a lower emission signal in fluorescence measurements. At 343 K, the mixtures show a counter wise behaviour for EtOH0 with the lowest absorption and

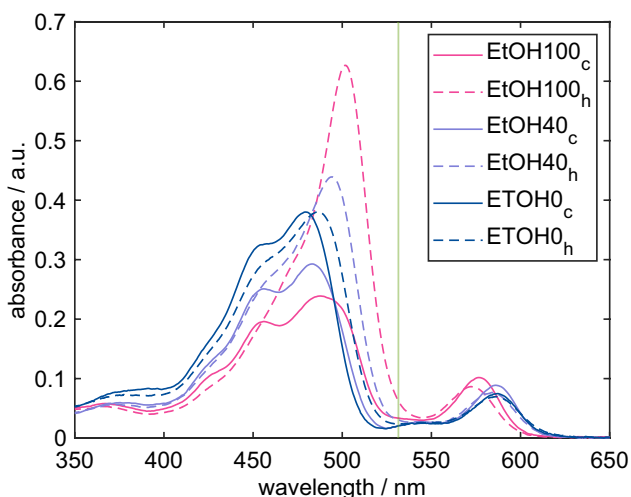


Fig. 2 Absorption spectra of different solvents at temperatures between 283 K (“c”-cold) and 343 K (“h”-hot). The laser line at 532 nm is depicted in green

EtOH100 with the highest. Nevertheless, the absorption rises with temperature in all solvent mixtures. Contrary to the temperature dependence of the FL peak, absorption of SRh in pure ethanol (EtOH100) is lower, the higher the temperature. Also opposing to FL is the shift of the SRh absorption peak towards longer wavelengths with rising water fraction. Due to shifting from the laser line at 532 nm, this trend may be responsible for lower emission signals of the second color channel in watery solvents.

3.2 Fluorescence spectroscopy: droplet size dependency

In the authors previous work, only 100 μm-sized droplets were considered. To show the applicability of the two-dye two-color approach to the complete size range of the droplet generator, measurements were conducted with droplets sized from 30 μm to 120 μm. This data was recorded in spherical droplets—depending on the droplet size and according settings this was at a distance of 2 mm to 4 mm below the nozzle exit. Figure 3 shows fluorescence emission spectra measured in 40 μm and 100 μm sized EtOH100 droplets, both at 293 K and 343 K. The signal reduces with the size of the droplets. For a better comparison, the spectra are normalized to their maximum. In all measurements, the VIS emission spectrum starts at around 490 nm to about 740 nm. A mounted notch filter blocks light around 532 nm to avoid over-exposure due to Mie scattering. The respective blocked wavelength band lies directly in the emission peak of FL. The greenish shaded area visualizes the temperature-dependent color channel. The shaded red color band covers an excerpt of the comparably temperature-insensitive SRh emission, with a peak maximum at 594 nm. A third peak around 649 nm can be observed in the spectra. This peak is due to lasing effects (or MDR) at the droplet rim.

The normalized spectra of the different droplet sizes reveal only little divergence in the emission peak of FL, with a slight red-shift of the big droplets’ spectra visible in the anti-stokes spectrum probably due to reabsorption. The wavelength region of the SRh peaks shows a match of the normalized spectra of both droplet sizes. The resulting calibration curves are depicted in the right graph in Fig. 3. Previous studies showed a linear behaviour of the

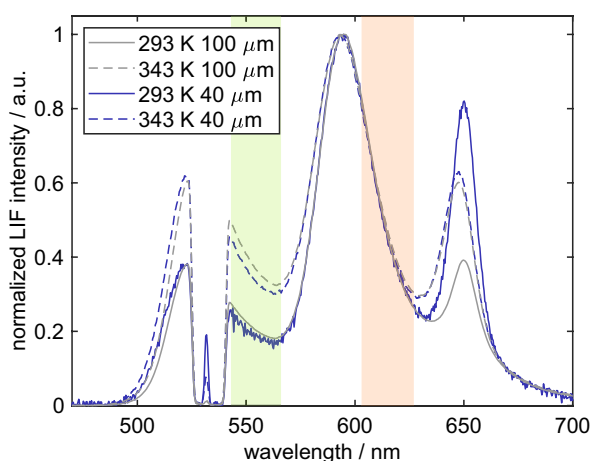
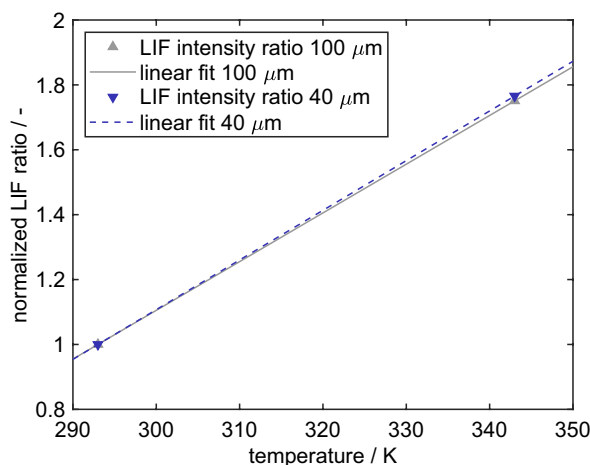


Fig. 3 Left: Normalized fluorescence emission spectra of the dye mixture detected in 40 μm (purple) and 100 μm (grey) sized ethanol droplets. Solid curves are for 293 K, dashed curves for 343 K. The shaded areas visualize the color channels, each representing the pass-



ing band of the respective BP filters in the imaging setup. Right: Normalized calibration curve of the LIF ratios received from respective spectra in the left image

temperature-dependent signal ratio, determined at seven temperatures between 283 and 343 K (Ulrich et al. 2023). The linear behaviour in this temperature range was found for ethanol, water and butanol droplets with a size of 100 μm (Ulrich and Zigan 2023), but the temperature sensitivity is slightly different for the three solvents. Thus, in order to show the influence of droplet size on the temperature sensitivity, calibration curves are fitted to only two calculated ratios, at 293 K and 343 K. In this experiment, measurements in both droplet sizes reveal a temperature sensitivity of the LIF signal ratio of 1.5%/K. To proof that MDR would not affect the temperature sensitivity of the chosen signal ratio, the position of the MDR peaks is detected in the measurements with droplet size variation. This study shows that the whole range of produced structure sizes can be processed further without the risk of influence on the intensity ratio by MDR.

3.3 Thermometry in an atomizing jet

To assess the suitability of the spectral detection system of the setup for, e.g. spray applications, temperature measurements downstream the droplet generator are conducted. Adjusting the droplet generator settings to a large volume flow, spray-like behaviour of the liquid flow is enforced. Reynolds, Weber and Ohnesorge numbers are estimated in the following section based on jet and droplet information rather than nozzle specifications, as the exact nozzle geometry and flow information is not available. These dimensionless numbers are crucial to describe the primary droplet breakup. The liquid Reynolds number Re_L represents the ratio of inertial forces to viscous forces and is defined by $Re_L = \rho \cdot v \cdot l / \eta$. For the calculation, the liquid-specific properties density ρ and dynamic viscosity η , as well as the velocity v and the specific length l are relevant. The liquid Weber number We_L serves as a stability criterion for jets and droplets and describes the ratio of inertial force to surface tension. Therefore, it additionally includes the surface tension σ as a relevant parameter: $We_L = \rho \cdot l \cdot v^2 / \sigma$. Representing a ratio of viscous forces to inertial and surface forces, the Ohnesorge number Oh is a combination of the Weber and Reynolds number and can be calculated by $Oh = \eta \cdot (l \cdot \rho \cdot \sigma)^{-0.5} = We_L^{0.5} / Re_L$. The length scale l corresponds to the jet or droplet diameter, respectively, determined by the LIF images. In the spray, different structure sizes are created, which are both in and out of focus so that the size cannot always be determined reliably with the imaging setup. With the spectral measurement approach, the challenges of differently sized liquid structures and depth of focus should be resolved. The jet is transient and the generated liquid structures are not reproducible regarding their form and shape. Five spectra (each 100 averaged, 50 ms integrated) are recorded at six different distances to the nozzle

exit. Three different injection settings were studied, showing a difference in set temperature at the nozzle and a difference in the liquid volume flow rate. Exemplary measurements are conducted in ethanol. To give an insight to the structure of the created spray, excerpts in form of single images, detected in the SRh color channel, are shown in Fig. 4. For each setting, recordings at the nozzle exit (0 mm), at a distance of 6 mm and 15 mm to the nozzle, are presented. For the first setting (left column), the volume flow rate was set to 15 ml/h and the initial temperature to 293 K. Both other measurements are investigated at an initial temperature of 343 K, one with a liquid flow rate of 15 ml/h (column 2) and the other one of 5 ml/h (column 3). All LIF images are displayed with the same color scale. For a better visibility of droplets at all temperatures, images detected in the temperature-insensitive LIF channel (SRh emission) are shown. This means that the temperature only hardly, but rather the droplet size, affects the signal. Using the initially described dimensionless numbers Re_L and Oh , the jet breakup regime can be estimated according to Ohnesorge (Ohnesorge 1936). The results are depicted in Table 1. With increase in liquid temperature at constant liquid flow, both Reynolds and Weber number rise, since viscosity and surface tension are reduced. A decrease in liquid volume flow leads to lower Reynolds- and Weber

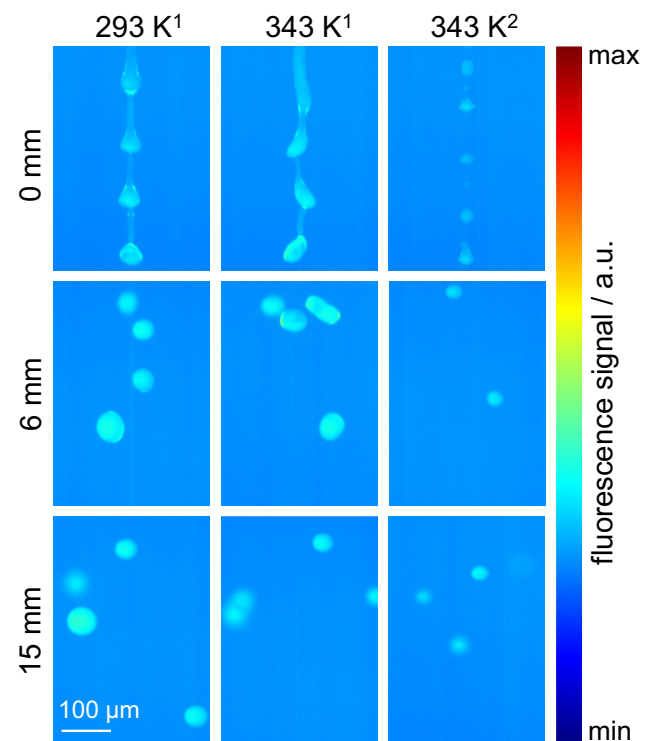


Fig. 4 Single images of the breaking up jet or droplet chain at three different distances downstream the nozzle exit. Temperatures of the droplet generator are set to 293 K and 343 K. LIF images depict the temperature-insensitive SRh color channel. Liquid volume flow rate: ¹15 ml/h, ²5 ml/h

Table 1 Dimensionless numbers Re_L , We_L and Oh of the three investigated ethanol jets. Respective fluid properties are extracted from (Dean and Lange 1999; FLUIDAT® on the Net 2024)

	293 K ¹	343 K ¹	343 K ²
Re_L	251.25	435.26	85.63
We_L	73.03	83.28	2.98
Oh	0.36	0.65	0.62
Jet breakup regime	2nd wind-induced	1st wind-induced	1st wind-induced

numbers at constant liquid temperature. All three studied cases are in the “wind-induced” regime.

In the first column, relatively large droplets are periodically released with a droplet diameter of around 39 μm and are subsequently dispersed due to the turbulent gas flow induced by the droplet stream. At increased temperature (central column), a liquid jet is visible at the nozzle outlet, which breaks up into longitudinally stretched droplets with an average diameter of about 35 μm at 6 mm distance to the nozzle exit. The reduced droplet sizes can be explained by the larger Weber numbers. Smaller surface tension may lead to more instable and deformed droplets at similar flow velocities, which tend to a decrease in breakup time. Further downstream the droplets are more dispersed and may show droplet collision and coalescence as well. In the third row at decreased liquid volume flow, smaller droplets with a diameter of about 23 μm are periodically generated forming a droplet chain and some very small (average of 11.3 μm) “satellite” droplets in between are visible. It should be noted that the smaller droplets compared to the previous cases are due to the lower liquid mass flow while the flow focussing air flow is kept constant, which is responsible for setting the initial droplet size inside the droplet generator. An increase in the droplet distance and droplet dispersion is visible further downstream (about 30 μm average diameter at 6 mm distance to the nozzle). At 15 mm, all images show “sharp” in-focus droplets and some blurred droplets are out of focus.

Spectra are being recorded at all three settings, post-processed and signal ratios are formed. Temperatures are obtained, using the calibration curve of the droplet chain measurements. The temperature progression downstream the nozzle exit is depicted in Fig. 5, recorded at all three settings. Two y-axes are shown to provide a better temperature resolution. The left, blue axis corresponds to the blue curve, showing the heat-up of the liquid jet at 293 K injected to ambient air at 296.2 K. Exiting the droplet generator, an initial temperature of 292.3 K is recorded. A temperature rise to 296.1 K at 10 mm after the nozzle exit is plausible, considering the higher ambient temperature. Furthermore, a cooling down to 294.8 K is observed between 10 and 20 mm distance to the nozzle exit, which can be explained

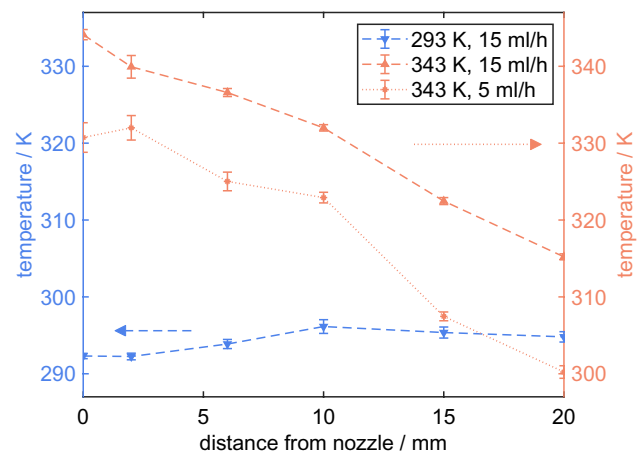


Fig. 5 Temperature progression measured downstream the nozzle exit. Two y-axes offer a better resolution of the temperature course. Blue (left axis): Liquid and air flow are tempered to 293 K. Red (right axis): Liquid and air flow are tempered to 343 K. Different liquid mass flows are measured

by evaporation cooling. These small temperature differences are in the same range as the shot-to-shot variations (maximum of 0.9 K at 10 mm distance) and could thus also result from measurement uncertainties.

The right, red y-axis relates to the two measurements with a set temperature of 343 K in the droplet generator. For both hot jets, being injected into ambient air, a cooling down of around 30 K is measured for the considered 20 mm distance. The first measurement is recorded with the same liquid volume flow (15 ml/h) as in the “cold” measurement. A liquid temperature of 344.1 K is measured at the exit of the droplet generator. A steady decrease of 28.9 K is measured within 20 mm due to convective cooling of the hot droplets by the cold ambient air and evaporation cooling. To further assess the origin of the temperature change, the lumped capacitance model was used to estimate the effect of heat transfer with the ambience. The dimensionless Biot number Bi expresses the instationary cooling or heating behaviour by relating the heat transfer coefficient h between liquid and surrounding to the thermal conductivity λ_L of the liquid: $Bi = h \cdot l / \lambda_L$ (Bergman et al. 2013). For small Biot numbers, a relatively homogeneous droplet temperature can be assumed, which is true for the present cases as well. Here, the Biot numbers are around 0.1 (0.09 to 0.13). A more detailed description of the procedure can be found in the appendix of the paper. For the hot case with 15 ml/h volume flow, approximately 4.6 K of the 29 K temperature reduction within 20 mm (corresponding to 2.2 ms) measurement distance are due to convective heat transfer with the ambience.

Smaller droplets and liquid structures are generated with a liquid volume flow of 5 ml/h. The setting of the focussing air is similar, which leads to higher evaporation rate at a lower liquid flow. The images in Fig. 4 show single droplets

exiting the nozzle, whereas a liquid jet is visible at the other settings. The droplets have a temperature of 330.7 K at the nozzle exit. Measurements at 2 mm distance to the exit reveal an initial increase of 1.2 K. This temperature rise could be explained by measurement uncertainties due to fluorescence light reflections close to the droplet generator surface. This theory was discussed in more detail in our previous work (Ulrich et al. 2023). Further downstream the spray, a decrease of 30.5 K is recorded for a distance of 18 mm. Considering the smaller droplet size compared to the other “hot” setting with 15 ml/h volume flow, the lower resulting temperatures and the slightly higher-temperature difference over the recorded 20 mm are reasonable. On the one hand, this can be explained by more efficient convective cooling. The larger droplets on the other hand have a larger thermal energy and the cooling is slower. Calculations of the cooling due to heat transfer of 17.7 K confirm the increased temperature reduction of the small droplets.

Furthermore, the temperature reduction induced by evaporation cooling is expected in the order of minimum 10 K. A numerical simulation of isolated ethanol droplets predicted a temperature reduction of about 17 K. The initial droplet and ambient temperature were 293 K and the droplet sizes were in the range of 5 μm to 40 μm , but the flow velocity was much higher (20 m/s) (Koeogl et al. 2020a, b, c, d). It should be noted that this simulation is a worst-case scenario and cannot be directly compared to the spray-like conditions in the present study.

Overall, only very little deviations (maximum of 1.9 K measured at the nozzle exit) are obtained within the spray measurements. These deviations arise from the five measured spectra, each consisting of 100 single spectra. Divergences due to different structure sizes and liquid structures out of focus are expected, but could not be observed so far.

3.4 Possibility of 2c-LIF and 3c-LIF for determination of the mixture composition

Apart from thermometry, the 2c-LIF approach can be used to investigate the mixture composition in fluids. Therefore, the dye emission has to spectrally shift, depending on the solvent. To verify the use of the proposed dye combination for determining the solvent mixture ratio, six different ethanol/water mixtures are investigated in the droplet chain. The emission spectra of these solvents, doped with FL and SRh, are shown in Fig. 6 on the left. In these measurements, 30 μm sized droplets were formed with the droplet generator and detected at around 2 mm below the nozzle exit. Due to the droplet shielding by the tempered focussing air, it is assumed that no distinct droplet temperature change nor vaporization takes place in the estimated 0.6 ms up until reaching the measurement position. For a better visibility of the spectral shift, all spectra are normalized to the maximum of the SRh peak. EtOH0 (water) droplets reveal the lowest signal and larger noise of all tested solvents. This can be explained by the lower absorbance of water at 532 nm compared to ethanol (see Fig. 2). The lower fluorescence signal for water compared to ethanol was also observed for other dyes such as Eosin-Y (Koeogl et al. 2020c). The FL spectrum, partially covered by the notch filter, reveals a blue-shift, the higher the water content. The SRh spectrum shifts contrary so that a red-shift is visible for higher water shares. This corresponds to the absorption spectra as shown in Fig. 2. Typically, the behaviour in absorption and fluorescence emission is similar. In general, a contradictory signal intensity behaviour in the two color channels is favourable for the use of an intensity ratio. In a first attempt, the same BP filters were taken in the liquid mixture investigation as in the

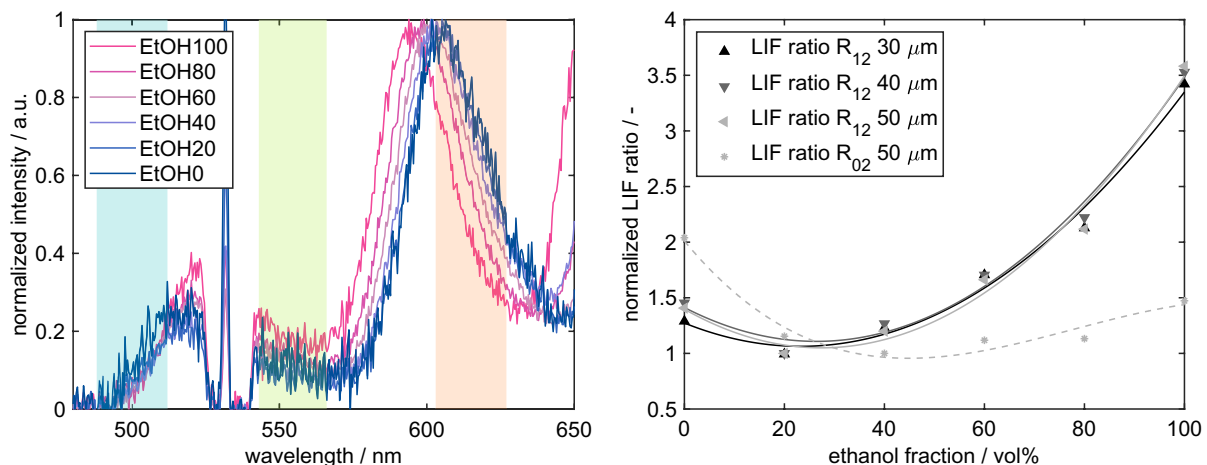


Fig. 6 Left: Fluorescence emission spectra of EtOH0 to EtOH100 in 30 μm sized droplets at 293 K. Shaded areas visualize the color channels (centre wavelengths at 500 nm (channel 0), 554 nm (channel

1) and 615 nm (channel 2)). Right: Calculated spectral LIF ratios of signal intensities of two color channels, each with the corresponding polynomial fit

Table 2 Characteristic properties of liquid ethanol at temperatures of 293 K and 343 K extracted from (FLUIDAT[®] on the Net 2024)

Ethanol properties		293 K	343 K
Kinematic viscosity ν	m ² /s	1.42·10 ⁻⁶	6.52·10 ⁻⁷
Density ρ	kg/m ³	804.9	747.3
Specific heat capacity c_p	J/kg·K	2409	2632
Thermal conductivity λ	W/m·K	1.69·10 ⁻¹	1.57·10 ⁻¹
Thermal diffusivity a	m ² /s	8.73·10 ⁻⁸	7.99·10 ⁻⁸
Surface tension σ	mN/m	22.39	18.23

Table 3 Characteristic fluid properties of air at temperatures of 293 K and 343 K extracted from (FLUIDAT[®] on the Net 2024)

Air properties		293 K	343 K
Kinematic viscosity ν	m ² /s	1.53·10 ⁻⁵	2.01·10 ⁻⁵
Density ρ	kg/m ³	1.19	1.02
Specific heat capacity c_p	J/kg·K	1009	1006
Thermal conductivity λ	W/m·K	2.60·10 ⁻²	2.95·10 ⁻²
Thermal diffusivity a	m ² /s	2.17·10 ⁻⁵	2.89·10 ⁻⁵

thermometry study in order to reduce effects of reabsorption and MDR.

The intensity ratio and a polynomial fit are depicted in the right graph for measurements of different ethanol–water mixtures in three differently sized droplets. The comparison of droplet sizes shows only a little divergence of the measurements in 30 μm droplets and mostly in EtOH0. This can be explained by the low signal detected in measurements with water. Diluted in this solvent, both fluorescent dyes absorb less photons, which decreases the probability of an emission event in the molecules. Additionally, the detection of 30 μm water structures represents the limit of both—the spectral and imaging—detection system (results are not shown here). This can be seen by very low signal intensities and thus, higher signal-to-noise ratios (SNR). The comparison of different droplet sizes shows, however, that despite the low signals similar results are achieved for all liquid mixtures studied.

As for the composition dependence, a higher LIF intensity ratio can be observed for increasing ethanol content. This correlation is valid for mixtures with ethanol fractions over 20 vol% and can be used for respective water–ethanol blends. To apply this measurement approach to mixtures with ethanol portions below 20 vol%, the ratio is not sufficient and another measurable variable has to be used, e.g. the location of a spectral maximum. In this case, the dependence of the SRh maximum is similar to the course of the second color channel and offers only little sensitivity at low ethanol fractions. Another possibility is the use of a third wavelength region for three-color LIF. Therefore, another third color channel at a lower wavelength is selected (according

to bandpass filter 500/24 BrightLine HC) and an additional LIF ratio is formed. With this additional information, a definite allocation of the ethanol portion can be performed by solving the two-equation system. This concept is further explained by Maqua et al. (2006) for PMT measurements in ethanol/acetone mixtures. An evaluation showed that the ratio R_{02} of the second and an additional color channel (0) in the spectrum of FL has a strong dependence on the ethanol content in mixtures with high water fraction (EtOH0 to EtOH40), as depicted by the dashed curve in Fig. 6 (right). It should be noted that the ratios R_{02} and R_{12} are both dependent on temperature and composition, so that a simultaneous planar measurement of these two quantities needs an iterative solution and further calibration data. For example, in (Ulrich and Zigan 2023) it was shown that the slopes of the temperature calibration curves R_{12} in pure ethanol and water are slightly different. However, it appears feasible to perform simultaneous spectral measurements of thermometry and composition. For this purpose, the concentration measurements can be conducted via the analyzation of the shift of the SRh spectrum in the “red” color channel, which hardly depends on temperature. A spectral fit algorithm is capable to provide information on the mixture composition, but further calibration at smaller temperature and concentration intervals is required.

4 Conclusion and outlook

This work concentrates on the first-time application of a two-dye 2c-LIF approach for thermometry in a droplet chain and atomizing jets with droplets sizes below 50 μm . The dyes, such as FL and SRh, are dissolved in various ethanol/water mixtures and detected with a spectrometer setup. For size calibration and insights into the behaviour of the droplets, an additional imaging setup records the fluorescence emission of the droplets. The focus of the detection lies on the spectral setup, as it has many advantages regarding size, cost and post-processing especially for technical systems with small optical access. Additionally, the occurrence of interference effects such as MDR can be monitored and the respective wavelength regions can be directly determined. Two intensity regions of the spectra are selected to form a temperature-sensitive ratio. These color channels are adopted from the respective bandpass filters with centre wavelengths at 554 nm and 615 nm, which were used for the camera system. Measurements of differently sized droplets between 30 μm and 120 μm demonstrate comparable temperature sensitivities of the intensity ratio. In the studied wavelength range and operating conditions, no influence of droplet size on the spectra and also lasing effects in the droplets (MDR) could be identified. This allows for subsequent atomizing jet measurements using the adjusted droplet generator. Thus,

Table 4 Equations for a step-by-step calculation of the droplet temperature due to contribution of convective heat transfer. For more detailed fundamentals of the model description and the calculations, see (Bergman et al. 2013; Ranz and Marshall 1952)

	293 K ¹	343 K ¹	343 K ²
Biot number $Bi = h \cdot l / \lambda_L$	0.12	0.13	0.09
Heat transfer coefficient $h = Nu_L \cdot \lambda_g / d_b$	3249.35	4021.92	4823.48
Nusselt number (laminar) $Nu_L = 2 + 0.664 \cdot Re_G^{1/2} \cdot Pr^{1/3}$ for $0 \leq Re_G < 200$ $0 \leq Pr \leq 250$	4.86	4.21	2.98
Reynolds number (gas) Re_G	23.43	14.10	2.77
Prandtl number Pr	0.70	0.70	0.70
Fourier number $ Fo = a_L \cdot t / r_D^2$			
Droplet temperature $ T = \exp(-Bi \cdot Fo) \cdot \Delta T + T_\infty$			

various droplet sizes were produced, which are located in- and outside of the detection focus of the imaging system. Successful temperature recordings downstream the jet were taken for three settings at two different temperatures and two different liquid volume flows. Within the measured distance of 20 mm, a cooling of about 29 K was obtained for the jet with an initial temperature set to 343 K and average droplet size of 35 μm (at 6 mm distance to the nozzle exit). A slightly larger temperature decrease of 30.5 K was measured for the jet with a lower liquid flow rate and thus smaller droplets with an initial average size of about 18 μm (at the nozzle exit). In the third setting, droplets were tempered to 293 K and a temperature increase of 3.8 K (to 296.2 K ambient air) was recorded.

Apart from the thermometry application, the use of the dye couple for 2c-LIF composition studies in ethanol/water mixtures was considered. For this purpose, a composition-dependent calibration curve was generated with the same color channels as used for thermometry. This allows the identification of ethanol fractions in mixtures with an ethanol content higher than 20 vol%. To enable the determination of smaller ethanol fractions, a third color channel, according to a bandpass filter for imaging, was proposed. Forming a second intensity ratio, the two calibration curves show a promising method for detecting composition dependence, each in a different range of ethanol fraction.

Future work should explore broader excerpts of typical industrial sprays, focussing less on microscopic droplet details and more on macroscopic spray formations and behaviour. Subsequent measurements are necessary to refine the ethanol fraction dependence of the 3c-LIF method. Furthermore, the combination with the thermometry approach would give huge benefits for solvent mixture investigations and should therefore be studied further. Simultaneous planar measurements of these two quantities require an iterative approach and additional calibration data. However, conducting simultaneous spectral measurements of thermometry and composition seems achievable. Concentration measurements can be realized by analysing the shift in the SRh spectrum within the "red" color channel, which is hardly affected by temperature. A spectral fitting algorithm can offer insights into mixture composition, although further calibration is needed at smaller temperature and concentration intervals. Investigations of the application on other solvent mixtures, such as propanol, butanol and water with varied pH value, would be beneficial.

Appendix

Fundamentals of the lumped capacitance model, used to estimate the temperature change in the droplet due to convective heat transfer with the surrounding, are provided

subsequently. Properties with the subscript “L” refer to the liquid, which in this case is ethanol. All relevant liquid properties necessary for the calculations can be found in Table 2.

As the ambient gas is air (subscript “G” for gas), the following Table 3 provides its main fluid properties at both investigated temperatures.

A step-by-step solution of the equations used to calculate the Biot numbers Bi as described in Sect. 3.3 can be obtained in the following overview (Table 4). In detail, Bi is estimated by a heat transfer coefficient h , which includes the Nusselt number Nu . In case of a laminar flow around a sphere (droplet, subscript “D”), Nu can be correlated empirically, which is valid for a specific range of gas-phase Reynolds numbers Re_G and Prandtl numbers Pr (Ranz and Marshall 1952). The values for both characteristic numbers are also listed in the table.

To further assess the temperature reduction by heat conduction and convection, the Fourier number Fo is evaluated, including the droplet radius r_D and a respective residence time t , which is estimated from the initial liquid volume flow. Finally, by means of Bi and Fo , the current average droplet temperature T can be estimated.

Acknowledgements The authors gratefully acknowledge funding of the Erlangen Graduate School in Advanced Optical Technologies (SAOT) by the Bavarian State Ministry for Science and Art. We thank the University of the Bundeswehr Munich for financial support. Open Access funding was enabled and organized by Project DEAL.

Author contributions HU and LZ conceptualized the experiment. HU designed the experiment and performed it together with RW. HU performed the data evaluation. HU wrote the paper. LZ performed funding acquisition and reviewed and edited the paper. All authors have read and agreed to the published version of the manuscript.

Funding Open Access funding enabled and organized by Projekt DEAL. The authors gratefully acknowledge funding of the Erlangen Graduate School in Advanced Optical Technologies (SAOT) by the Bavarian State Ministry for Science and Art. We thank the University of the Bundeswehr Munich for financial support. Open Access funding was enabled and organized by Project DEAL.

Data availability Data can be shared upon request.

Declarations

Conflict of interest The authors declare no competing interests.

Open Access This article is licensed under a Creative Commons Attribution 4.0 International License, which permits use, sharing, adaptation, distribution and reproduction in any medium or format, as long as you give appropriate credit to the original author(s) and the source, provide a link to the Creative Commons licence, and indicate if changes were made. The images or other third party material in this article are included in the article’s Creative Commons licence, unless indicated otherwise in a credit line to the material. If material is not included in the article’s Creative Commons licence and your intended use is not permitted by statutory regulation or exceeds the permitted use, you will need to obtain permission directly from the copyright holder. To view a copy of this licence, visit <http://creativecommons.org/licenses/by/4.0/>.

References

- Amyrgialaki E, Makris DP, Mauromoustakos A, Kefalas P (2014) Optimisation of the extraction of pomegranate (*Punica granatum*) husk phenolics using water/ethanol solvent systems and response surface methodology. *Ind Crops Prod* 59:216–222. <https://doi.org/10.1016/j.indcrop.2014.05.011>
- Bergman TL, Incropera FP, DeWitt DP, Lavine AS (2013) Principles of heat and mass transfer. Wiley
- Bhatt NH, Lily RR, Varshney P, Pati AR, Chouhan D, Kumar A, Munshi B, Mohapatra SS (2017) Enhancement of heat transfer rate of high mass flux spray cooling by ethanol-water and ethanol-tween20-water solution at very high initial surface temperature. *Int J Heat Mass Transf* 110:330–347. <https://doi.org/10.1016/j.ijheatmasstransfer.2017.02.094>
- Bräuer A (2015) In situ spectroscopic techniques at high pressure, vol 7. Elsevier, Amsterdam
- Capello C, Fischer U, Hungerbühler K (2007) What is a green solvent? A comprehensive framework for the environmental assessment of solvents. *Green Chem* 9(9):927. <https://doi.org/10.1039/b617536h>
- Castanet G, Lavieille P, Lebouch M, Lemoine F (2003) Measurement of the temperature distribution within monodisperse combusting droplets in linear streams using two-color laser-induced fluorescence. *Exp Fluids* 35(6):563–571. <https://doi.org/10.1007/s00348-003-0702-1>
- Chaze W, Caballina O, Castanet G, Lemoine F (2016) The saturation of the fluorescence and its consequences for laser-induced fluorescence thermometry in liquid flows. *Exp Fluids* 57(4):1–18. <https://doi.org/10.1007/s00348-016-2142-8>
- Chaze W, Caballina O, Castanet G, Lemoine F (2017) Spatially and temporally resolved measurements of the temperature inside droplets impinging on a hot solid surface. *Exp Fluids* 58(8):1–16. <https://doi.org/10.1007/s00348-017-2375-1>
- Chemat F, Abert Vian M, Ravi HK, Khadhraoui B, Hilali S, Perino S, Tixier A-SF (2019) Review of alternative solvents for green extraction of food and natural products: panorama, principles, applications and prospects. *Molecules*. <https://doi.org/10.3390/molecules24163007>
- Collignon R, Caballina O, Lemoine F, Castanet G (2021) Temperature distribution in the cross section of wavy and falling thin liquid films. *Exp Fluids*. <https://doi.org/10.1007/s00348-021-03175-x>
- Collignon R, Caballina O, Lemoine F, Castanet G (2022) Simultaneous temperature and thickness measurements of falling liquid films by laser-induced fluorescence. *Exp Fluids*. <https://doi.org/10.1007/s00348-022-03420-x>
- Dean JA, Lange NA (1999) Lange’s handbook of chemistry, vol 15. McGraw-Hill, New York
- Düwel I, Ge H-W, Kronemayer H, Dibble R, Gutheil E, Schulz C, Wolfrum J (2007) Experimental and numerical characterization of a turbulent spray flame. *Proc Combust Inst* 31(2):2247–2255. <https://doi.org/10.1016/j.proci.2006.07.111>
- Dzigbor A, Chimphango A (2019) Evaluating the potential of using ethanol/water mixture as a refrigerant in adsorption cooling system by using activated carbon–sodium chloride composite adsorbent. *Int J Refrig* 97:132–142. <https://doi.org/10.1016/j.ijrefrig.2018.09.025>
- FLUIDAT® on the Net (2024) FLUIDAT® (V1.86). Bronkhorst High-Tech B.V
- Koegl M, Mishra YN, Baderschneider K, Conrad C, Lehnert B, Will S, Zigan L (2020a) Planar droplet sizing for studying the influence of ethanol admixture on the spray structure of gasoline sprays. *Exp Fluids*. <https://doi.org/10.1007/s00348-020-03040-3>
- Koegl M, Mull C, Mishra YN, Will S, Zigan L (2020b) Characterization of fuel/water mixtures and emulsions with ethanol using

- laser-induced fluorescence. *Appl Opt* 59(4):1136–1144. <https://doi.org/10.1364/AO.380392>
- Koegl M, Pahlevani M, Zigan L (2020c) A novel approach for measurement of composition and temperature of n-decane/butanol blends using two-color laser-induced fluorescence of Nile Red. *Sensors* 20(19):5721. <https://doi.org/10.3390/s20195721>
- Koegl M, Weiß C, Zigan L (2020d) Fluorescence spectroscopy for studying evaporating droplets using the dye eosin-Y. *Sensors (basel Switzerland)*. <https://doi.org/10.3390/s20215985>
- Koegl M, Dai H, Baderschneider K, Ulrich H, Zigan L (2022) Polarization-dependent LIF/Mie ratio for sizing of micrometric ethanol droplets doped with Nile red. *Appl Opt* 61(14):4204–4214. <https://doi.org/10.1364/AO.457685>
- Koegl M, Milto N, Zigan L (2024) Simultaneous film temperature and film thickness measurements for jet impingement applications using two-color laser-induced fluorescence. *Exp Fluids*. <https://doi.org/10.1007/s00348-024-03782-4>
- Lache M, Kappelhoff C, Seiler J, Bardow A (2023) Water and ethanol as refrigerant mixture enabling adsorption cooling below 0 °C. *Energy Technol*. <https://doi.org/10.1002/ente.202201158>
- Lavielle P, Lemoine F, Lavergne G, Lebouché M (2001) Evaporating and combusting droplet temperature measurements using two-color laser-induced fluorescence. *Exp Fluids* 31(1):45–55. <https://doi.org/10.1007/s003480000257>
- Lemoine F, Castanet G (2013) Temperature and chemical composition of droplets by optical measurement techniques: a state-of-the-art review. *Exp Fluids* 54(7):1–34. <https://doi.org/10.1007/s00348-013-1572-9>
- Lemoine F, Antoine Y, Wolff M, Lebouche M (1999) Simultaneous temperature and 2D velocity measurements in a turbulent heated jet using combined laser-induced fluorescence and LDA. *Exp Fluids* 26(4):315–323. <https://doi.org/10.1007/s003480050294>
- Maqua C, Castanet G, Lemoine F, Doué N, Lavergne G (2006) Temperature measurements of binary droplets using three-color laser-induced fluorescence. *Exp Fluids* 40(5):786–797. <https://doi.org/10.1007/s00348-006-0116-y>
- Mishra YN, Abou Nada F, Polster S, Kristensson E, Berrocal E (2016) Thermometry in aqueous solutions and sprays using two-color LIF and structured illumination. *Opt Express* 24(5):4949–4963. <https://doi.org/10.1364/OE.24.004949>
- Mishra YN, Yoganantham A, Koegl M, Zigan L (2020) Investigation of five organic dyes in ethanol and butanol for two-color laser-induced fluorescence ratio thermometry. *Optics* 1(1):1–17. <https://doi.org/10.3390/opt1010001>
- Monroy YM, Rodrigues RA, Sartoratto A, Cabral FA (2016) Influence of ethanol, water, and their mixtures as co-solvents of the supercritical carbon dioxide in the extraction of phenolics from purple corn cob (*Zea mays* L.). *J Supercrit Fluids* 118:11–18. <https://doi.org/10.1016/j.supflu.2016.07.019>
- Mylonaki S, Kiassos E, Makris DP, Kefalas P (2008) Optimisation of the extraction of olive (*Olea europaea*) leaf phenolics using water/ethanol-based solvent systems and response surface methodology. *Anal Bioanal Chem* 392(5):977–985. <https://doi.org/10.1007/s00216-008-2353-9>
- Najim M, Feddaoui M, Nait Alla A, Charef A (2020) Channel wall cooling by evaporative falling water-ethanol and water-methanol films. *Heat Transfer Eng* 41(18):1596–1608. <https://doi.org/10.1080/01457632.2019.1661688>
- Ohnesorge WV (1936) Die bildung von tropfen an düsen und die auflösung flüssiger strahlen. *ZAMM–J Appl Math Mech* 16(6):355–358. <https://doi.org/10.1002/zamm.19360160611>
- Palmer J, Reddemann MA, Kirsch V, Kneer R (2016) Temperature measurements of micro-droplets using pulsed 2-color laser-induced fluorescence with MDR-enhanced energy transfer. *Exp Fluids* 57(12):1–14. <https://doi.org/10.1007/s00348-016-2253-2>
- Perrin L, Castanet G, Lemoine F (2015) Characterization of the evaporation of interacting droplets using combined optical techniques. *Exp Fluids* 56(2):1–16. <https://doi.org/10.1007/s00348-015-1900-3>
- Plaskova A, Mlcek J (2023) New insights of the application of water or ethanol-water plant extract rich in active compounds in food. *Front Nutrition*. <https://doi.org/10.3389/fnut.2023.1118761>
- Prenting MM, Bin Dzulfida MI, Dreier T, Schulz C (2020) Characterization of tracers for two-color laser-induced fluorescence liquid-phase temperature imaging in sprays. *Exp Fluids* 61(3):1–15. <https://doi.org/10.1007/s00348-020-2909-9>
- Qi DH, Chen H, Matthews RD, Bian Y (2010) Combustion and emission characteristics of ethanol–biodiesel–water micro-emulsions used in a direct injection compression ignition engine. *Fuel* 89(5):958–964. <https://doi.org/10.1016/j.fuel.2009.06.029>
- Ranz WE, Marshall WR (1952) Evaporation from Drops. *Chem Eng Prog* 48(3):141–146
- Schulz C, Sick V (2005) Tracer-LIF diagnostics: quantitative measurement of fuel concentration, temperature and fuel/air ratio in practical combustion systems. *Prog Energy Combust Sci* 31(1):75–121. <https://doi.org/10.1016/j.pecs.2004.08.002>
- Storch M, Lind S, Will S, Zigan L (2016a) Influence of ethanol admixture on the determination of equivalence ratios in DISI engines by laser-induced fluorescence. *Appl Opt* 55(30):8532–8540. <https://doi.org/10.1364/AO.55.008532>
- Storch M, Mishra YN, Koegl M, Kristensson E, Will S, Zigan L, Berrocal E (2016b) Two-phase SLIPI for instantaneous LIF and Mie imaging of transient fuel sprays. *Opt Lett* 41(23):5422–5425. <https://doi.org/10.1364/OL.41.005422>
- Strizhak PA, Volkov RS, Castanet G, Lemoine F, Rybdylova O, Sazhin SS (2018) Heating and evaporation of suspended water droplets: experimental studies and modelling. *Int J Heat Mass Transf* 127:92–106. <https://doi.org/10.1016/j.ijheatmasstransfer.2018.06.103>
- Taheri V, Ebrahimi Rahnama H, Morad MR (2024) High flow rate electrospray cooling performance of water–ethanol mixtures. *Appl Thermal Eng*. <https://doi.org/10.1016/j.applthermaleng.2023.122200>
- Ulrich H, Sigl S, Möhnle M, Berrocal E, Zigan L (2023) Droplet thermometry based on an optimized two dye two-color laser-induced fluorescence concept. *Front Physics*. <https://doi.org/10.3389/fphy.2023.1235847>
- Ulrich H, Zigan L (2023) Characterization of a Dye Mixture for Two-Color Laser-Induced-Fluorescence Thermometry in Ethanol, Butanol and Water Droplets and Sprays. (11th European Combustion Meeting)
- Volkov RS, Strizhak PA (2020) Using Planar Laser Induced Fluorescence to determine temperature fields of drops, films, and aerosols. *Measurement*, 153. <https://doi.org/10.1016/j.measurement.2019.107439>
- Zehentbauer FM, Moretto C, Stephen R, Thevar T, Gilchrist JR, Pokrajac D, Richard KL, Kiefer J (2014) Fluorescence spectroscopy of Rhodamine 6G: concentration and solvent effects. *Spectrochim Acta Part a, Mol Biomol Spectrosc* 121:147–151. <https://doi.org/10.1016/j.saa.2013.10.062>
- Zhang Z-S, Li D, Wang L-J, Ozkan N, Chen XD, Mao Z-H, Yang H-Z (2007) Optimization of ethanol–water extraction of lignans from flaxseed. *Sep Purif Technol* 57(1):17–24. <https://doi.org/10.1016/j.seppur.2007.03.006>

Publisher's Note Springer Nature remains neutral with regard to jurisdictional claims in published maps and institutional affiliations.